Upper Ocean Thermohaline Structure and its Temporal Variability in the Southeast Indian Ocean

Xiaojun Yuan[1] *and Douglas G. Martinson*

Lamont-Doherty Earth Observatory, Palisades, NY 10964

Zhaoqian Dong

Polar Research Institute of China, Shanghai, China

ABSTRACT

We examine the upper ocean thermohaline structure in the southeast Indian Ocean and its temporal variability based on XBT/XCTD observations from four cruises across the Southern Ocean from Fremantle, Australia to Prydz Bay, Antarctica. The transects were occupied in March 1998, November 1998, March 2000, and March 2002. Three major fronts: the subtropical front, subantarctic front and polar front, are clearly identified from our surveys and compared with earlier studies. Particularly, two polar fronts, separated by a few degrees of latitude, appear southeast the Kerguelen Plateau. The primary polar front is characterized by a strong horizontal thermal gradient extending deep in the water column, while the secondary polar front is identified by the 2˚C isotherm at T_{min} depth and has a relatively shallow frontal expression. Dynamic height across the Antarctic Circumpolar Current (ACC) was calculated for the transects in 2000 and 2002. With a negligible yearly variation in the total transport across the ACC, the higher sample density in 2002 reveals more detailed structure of the ACC: two jets associated with the subantarctic front and primary polar front are embedded within the broad ACC.

We find a strong temporal variation in the upper ocean thermal structure in the polar ocean southeast the Kerguelen Plateau. The depths of the mixed layer and T_{min} layer increase over time. The mixed layer temperature decreases while the T_{min} temperature increases during the same period. In addition, we see an increase from 1998 to 2002 in the length of the ice-free period prior to each XBT/XCTD sampling and surface wind forcing, calculated as the friction velocity cubed during the ice-free period. Our analysis suggests that the longer the ocean is exposed to the atmosphere and the stronger the wind stirring, the more enhanced is the turbulent mixing. This results in a greater mixed layer depth and more entrainment of colder water from the T_{min} layer to the mixed layer. This surface forcing also enhances internal diffusive processes that mix the T_{min} water with the warmer waters above and below the T_{min} layer. The surface forcing is apparently dominant in determining the upper ocean thermal structure in this polar region.

Key Words: Oceanic fronts, Polar front, Mixed layer, T_{min} layer, Interannual variability, Atmospheric forcing, The Southeast Indian Ocean (35˚ – 70˚S, 70˚ -110˚E).

1. Introduction

[1] Corresponding author. Tel: 845 365 8820; Fax: 845 365 8736; Email: xyuan@ldeo.columbia.edu

The Southern Ocean is an important component of global climate. Its circumpolar current plays a crucial role in the global transport of mass, heat and momentum, and transports climate signals from one ocean basin to another. The central/eastern Indian Ocean sector of the subpolar region has been shown to be anomalous, relative to other circumpolar regions in the following ways: in its relationship to extrapolar climate, and in apparently not propagating (Yuan and Martinson, 2000) the Antarctic Circumpolar Wave (White and Peterson, 1996), in the lack of long-term trends in the sea ice extent (Yuan and Martinson, 2000), in playing an important role in circumpolar large-scale cyclogenesis (Yuan et al. 1999), and in a number of regionally-specific physical characteristics (e.g., this is the region of farthest northward displacement of the Antarctic continent excepting the Antarctic Peninsular, with unusually close proximity to the Antarctic Circumpolar Current).

Unfortunately the paucity of data prevents us from understanding the physical and dynamical processes that make the Southern Indian Ocean different from other basins. Particularly, time series are too short and too sparse to identify oceanic roles in the regional air-sea-ice coupled system from synoptic to interannual time scales, as well as to isolate the lead/lag nature of polar-extrapolar teleconnections. Based on historical hydrographic data, recent studies (Peterson and Stramma, 1991, Orsi et al., 1995; Belkin and Gordon, 1996) described large scale frontal distributions and water mass characteristics in the Southern Ocean. These extensive studies provide the general background of oceanic spatial conditions but not the temporal variability. The only Southern Indian Ocean time series were made from Japanese ships supplying Antarctic scientific bases. For more than three decades, Japanese scientists have been sampling temperature profiles in the upper 400 meters annually with XBT (MBT in early years) probes along the cruise tracks of the supply ships. These series revealed that the position of major fronts varied interannually (Nagata et al., 1988) and that a long-term trend and 4-5 year cycle variability were present in the upper ocean temperature field (Aoki, 1997). Another repeated XBT line east of the Japanese transects exits across the Antarctic Circumpolar Current (ACC) from Tasmania, Australia to the French Antarctic base Dumont d'Urville maintained by a collaboration among Australia, France and the United States (Rintoul et al., 1997, Rintoul et al., 2002). This repeated transit revealed seasonal variability in the upper ocean temperature and heat content, and variation of major fronts (Rintoul et al., 1997). Moreover, in the vicinity of this XBT line, a WOCE hydrographic section (SR3) has been repeated six times from 1991 to 1996 (Rintoul and Bullister, 1999). Rintoul and Sokolov (2001) have estimated mass, heat, salt and nutrient fluxes from these sections. Frontal variations from these sections were reported in Sokolov and Rintoul (2002).

Utilizing underway sampling conducted from the ships supplying Antarctic coastal stations has been shown to be a cost-effective way of sampling large data void regions in the Southern Ocean. China operates two Antarctic research stations: Zhongshan Station in Prydz Bay (69˚22'S, 76˚23'E) and Great Wall Station in King George Island (62˚13'S, 58˚58'). Chinese R/V Xuelong services Zhongshan Station every year and Great Wall station every other year. Since 1998, an US/Chinese collaboration has conducted yearly XBT/XCTD sampling in the Southern Indian Ocean along R/V Xuelong's cruise tracks from Fremantle, Australia to Prydz Bay. The observations expand the existing oceanic time series maintained by Japanese and Australia/US/France in the east. Particularly, the XCTD sampling provides better descriptions of water masses and better estimates of dynamic height since salinity is a crucial element in high latitude oceans. Our study describes the upper ocean temperature, salinity structures and dynamic height distribution based on four repeated sections occupied between 1998 and 2002. Variations of major fronts are compared with nearby Japanese surveys along 110˚E. Interannual variability of the upper ocean thermal structure is investigated in the polar ocean southeast of Kerguelen Plateau, together with the variability in surface winds and influence from the cryosphere.

2. Data

Four XBT/XCTD sections from Fremantle to Prydz Bay were occupied in March 1998, November 1998, March 2000 and March 2002. The earlier two cruises were designed as a pilot program to evaluate logistic and technical problems, so they were sampled at relatively coarse resolutions. The spatial resolution was increased substantially in the later two cruises. However, faulty probes and rough conditions caused significant gaps in these sections. Most XBTs sampled the upper 760 meters while XCTDs sampled the upper 1000 meters.

All XBT/XCTD profiles went through a careful quality control procedure guided by CSIRO Cookbook for Quality Control of Expendable Bathythermograph (XBT) Data

(1993). First, XBT positions and times were checked against sampling logs. Second, each XBT profile was examined to eliminate readily visible malfunctions such as consistent temperature, broken wire and obvious bad profiles due to faulty probes. Then, each XBT profile was examined for spikes caused by external electronic/electromagnetic interference and insulation penetration, temperature inversion due to wire stretch and leakage, etc. Isolated spikes were removed from profiles and data gapes were filled with a linear interpolation. We rejected profiles with high frequency spikes and large temperature inversions but accepted profiles with minor temperature inversions (< 0.2°C). Finally, waterfall plots for each XBT section were generated to further evaluate the consistency of these temperature profiles. The profiles with temperature offset were rejected in this process. XCTD profiles were quality-controlled in the same way. Since large amounts of high frequency noise exist in XCTD salinity profiles, a median filter with a filter width of 15m is applied to XCTD profiles. March and November climatologies for these regions (Conkright et al., 1998) are based on too few data to provide an additional means for quality control. Figure 1 shows the final data points.

Temperature distributions were produced using an objective mapping method (Roemmich, 1983) for all cruises except the cruise in March 1998 (red dots in Figure 1), in which the stations were too sparse. The largest gap in March 1998 reaches about 20 degrees of latitude near the Antarctic Circumpolar Current (ACC). XCTDs were deployed at a much lower spatial resolution, so salinity distributions along the cruise tracks were only objectively analyzed for the later two cruises.

NCEP/NCAR reanalysis (Kalnay et al., 1996) monthly surface winds at 10m were used to evaluate frontogenesis and upper ocean variability due to atmospheric forcing. Sea ice concentration data (Comiso, 1999) were also used to examine the winter ice cover's influence on the variability of the upper ocean temperature structure.

3. Water Masses and T/S Structures

The repeated XBT/XCTD sections cross three very different oceanic domains: the polar ocean, Subantarctic region and subtropical gyre. Several water masses are clearly apparent in these sections (Figure 2, 3, 4, 5). Following the classifications in earlier studies (Park et al., 1993; Orsi et al., 1995; Rintoul and Bullister, 1999; Sokolov and Rintoul, 2000), these include: (1) the subtropical surface water (STSW), characterized by high salinity water above 200 m depth; (2) the subantarctic surface water (SASW) which has temperature between 5˚ to 10˚C; and (3) the Antarctic surface water (AASW) which has temperature below 2˚C and salinity lower than 34.1 (on practical salinity scale, unit-less, Lewis, 1980, Perkin and Lewis, 1980). The STSW is found north of the subtropical front and the SASW is located between the subantarctic front and polar front, while the AASW with small horizontal and vertical gradients extends from the polar front to the Antarctic coast.

Below the AASW, temperature minimum layer (T_{min}) at approximately 100m indicates the winter mixed layer depth. The Upper Circumpolar Deep Water (UCDW), which is relatively saltier and warmer than the T_{min} layer, lies below the T_{min} and occupies a large area extending throughout the polar ocean to the subpolar/ACC regions. The Subantarctic Mode Water (SAMW) is identified in the subsurface (100-500m) as a thick, relatively uniform layer from latitude of 40˚ to 45˚S with a couple of degrees of interannual variability. The Antarctic Intermediate Water cannot be resolved due to the limited depth of the surveys.

4. Variability of Major Fronts

Fronts are usually identified by rapid horizontal changes in water properties. Many previous studies have given different criteria to identify frontal positions. Belkin and Gordon (1996, BG96 hereafter) provided extensive discussions on the numerous criteria that have been used to define the fronts in the South Atlantic and South Indian Ocean. For the purpose of comparison, we mainly adopted BG96 definitions for the three major fronts found in our sections.

4.1 The Subtropical Front (STF)

BG96 identified the south STF south of the Africa by the existence of the subsurface salinity maximum (S_{max}) south of the front, plus a sharp change of the surface salinity (S_0) across 35.0. These salinity characteristics clearly exist in our sections. Moreover, these salinity criteria coincide with a relatively high temperature gradient at the surface between the 13˚ and 15˚C isotherms in 2000 and 2002, indicating a separation of surface water masses. Therefore, we believed that the BG96 definition can be extended further east to our sections. The STF is identified in all three sections (Figure 3b,4b,5b) based on the temperature criterion. The frontal structure is quite similar in these three temperature sections although the frontal position may not be precise in 1998 due to the lower sampling density. Nagata et al.'s (1988) definition of T_{150}=12˚C will result in the same STF location that we found. The T-S range of this front (Table 1) is comparable to that of the BG96's south STF south of the Africa (0-40˚E), while the frontal location is slightly south of the BG96's south STF. However, the spatial variation of the STFs is consistent with that found in BG96 (Figure 6). The interannual variability of the STF position is quite small compared to the range of 36˚ to 42˚S found along 110˚E by Nagata et al. (1988). The STF falls in the climatological Ekman convergent zone.

3.2 The Subantarctic Front (SAF)

The SAF is identified by structural criteria defined as the existence of the intermediate salinity minimum (S_{min}) and the Subantarctic Mode Water (SAMW) thermostad north of the SAF (BG96). In the three temperature sections, the SAMW below the seasonal thermocline is clearly visible (Figure 3b,4b,5b). However, the intermediate S_{min} north of the SAF usually extends below 800m in this region (Figure 15 in BG96) and is not well established in our sections because of sampling depth (Figure 4c,5c). The SAMW is bounded to the south by a region with strong lateral temperature and salinity gradients extending from the surface to the full depth of the surveys. In 2000 these strong lateral gradients identify the SAF, located between 44˚ and 45˚S, for example. The temperature changes from 6˚ to 10˚C across the front below 200m for all three sections. This range is warmer than that observed along 110˚E by the Japanese (Nagata et al., 1988) and the temperature averaged in the Southern Ocean (Orsi et al. 1995). Salinity sampling is too sparse to locate the SAF precisely in the salinity sections; the salinity varies from 34.2 to 34.7 across the front. The SAF identified in 1998 and 2000 is a couple of degrees of latitude north of the BG96 SAF, while the SAF in 2002 is slightly south of the BG96 SAF (Figure 6). Again, the temporal variability of the SAF is quite small relative to that found by Nagata et al. (1988), who defined the SAF as T_{100}=7˚C. The frontal definition may contribute to the large variability in the front position since individual isotherms may have larger variation than the water mass structure itself. On the other hand, Nagata et al. (1988) had a time series of 22 years, giving more opportunity for larger variations. The SAF also falls in the climatological Ekman convergent zone.

3.3 The Polar Fronts (PF)

BG96 identified the PF by the northern terminus of the subsurface temperature minimum (T_{min}) layer bounded by the 2˚C isotherm in the 100-300 m depth range in a temperature section. Using these criteria, we identify the PF at 53.5˚S in November 1998 (Figure 3b). This location lies between stations, so the actual frontal location may vary slightly. The PF is found at 52.5˚S in March 2000 and 54.5˚S in March 2002 (Figure 4b,5b). The PF in 2000 is quite close to the BG96 PF location, though the PF in 1998 and 2002 is about 2-3 degrees of latitude south of the BG96 PF (Figure 6). The interannual spatial variability of the PF from the Japanese transects along 110˚E spans from 50˚ to 53˚S, which is also south of the BG96's PF (Figure 6).

The PF marked by the 2˚C isotherm at T_{min} layer usually has an increased lateral thermal gradient at the surface (Figure 3b,4b,5b) and has a shallow frontal expression in our sections. In addition, no lateral salinity gradient exists associated with this PF. Between the PF and the SAF exists another high temperature gradient zone extending to the full depth of the observation and forming a separate front. Since it marks the northern limit of T_{min} and bounds the upper circumpolar deep water to the south, we identify it as a polar front also, although Sokolov and Rintoul (2002) identified this front as a southern SAF in the region south of Australia. The isotherms of 3˚ to 6˚C are usually embedded in this northern polar front below 200m. The two PFs are separated by a few degrees of latitude particularly in November 1998 and March 2002. In these two sections, two separate high temperature gradient zones are clearly visible at the surface. There is no clear surface separation in 2000, although the 2˚C isotherm at T_{min} layer is still separated by a few degrees of latitude from the maximum temperature gradient below the 200m depth. The northern PF has a high salinity gradient below 400m (Figure 4c,5c). It occurs near the zero wind stress curl, suggesting that the wind driven circulation is likely the frontogenesis.

This double PF structure is apparently a regional phenomenon near some major topography. Sparrow et al. (1996) found the separate surface and sub-surface expressions of the PF near the Kerguelen Plateau just west of our XBT/XCTD transects. The separation of the two PFs reached as large as 8˚ latitude. A similar double PF structure was found as a permanent phenomenon in a limited region near the Macquarie Ridge south of New Zealand (Gordon, 1971). Gordon identified the deep-reaching northern PF as the primary polar front, and the front associated with the 2˚C isotherm at the T_{min} layer as the secondary polar front, we will adopt this convention here. Moreover, Moore et al. (1999) suggested a double PF structure in a limited region on the Falkland Plateau in the southern Atlantic based on sea surface temperature derived from satellites.

5. Dynamic Height

Dynamic height of the sea surface relative to 750m was calculated in 2000 and 2002 when the XCTD sample density was relatively high (Figure 7). The range of dynamic height between 40˚ and 60˚S does not vary much in these two years, and is in good agreement with Orsi et al. (1995) even though the reference level in Orsi et al. (1995) is about 200m deeper than ours. However, the transect in 2002 gives a more detailed structure due to a higher sample density. Two jets associated with the SAF (~45˚S) and primary PF (~52˚S) exist in the broad ACC current system. Figure 7c shows that density fronts associated with these two jets reach the full depth of the survey (~1000m). The surface current relative to 875m, which is the deepest reference level allowed in the 2002 survey, reaches a speed of 1 m/s within the two jets. Outside of these frontal jets, the mean ACC speed between 40˚S and 60˚S is about 0.2 m/s (not shown here).

6. Interannual Variability of Polar Upper Ocean

Since the cruise tracks of these four surveys didn't repeat each other exactly (Figure 1), it is difficult to examine the interannual variability of the water columns. Adding to the difficulty is the fact that one survey was conducted in November while the other three were conducted in March. In a few locations, three or four years of data are available to examine the interannual variability of upper ocean temperature. First, the northern end of the sections, where the cruise tracks merged, provided a location with small spatial variability. However, the section in 2000 didn't extend into this area. The remaining three surveys in this area were not conducted in the same season; the seasonality strongly contaminates the interannual signal. Second, the cruise tracks were relatively close to each other near the mid-ocean ridge, where data from all four sections are available. However, a strong lateral gradient exists in this area, introducing large noise into the interannual signal. Contrast this to the southern end of the sections (south of 60˚S) where three cruise tracks were quite close to each other, all were occupied in March, and the lateral gradient of the AASW is relatively small. For these reasons, we chose this region as a better place to examine the upper ocean interannual variability.

In a region south of the PF bounded by 60˚-64˚S and 78˚-83˚E, there were two, six and four temperature profiles in 1998, 2000 and 2002, respectively. The cruise tracks from 1998 and 2000 overlapped each other, while the cruise track in 2002 had about 2˚ longitude offset from earlier years (Figure 1), which would introduce near 0.2˚C lateral temperature changes at 50m depth based on the WOA98 data (Conkright et al., 1998). A shallow temperature-based mixed layer on the top of the subsurface Tmin characterizes the water column in this region in March (Figure 8). Averaging available temperature at each depth, we generated the mean temperature profile for each year. The large variation in the mixed layer (about 1.5˚C at 50m) and main thermocline below the T_{min} (about 0.7˚C at 100m) would generally reflect the interannual variability (Figure 9). This variability is comparable to the interannual variability in the nearby area between 90˚ and 130˚E, which was observed over a 12-year period by Aoki (1997). From 1998 to 2000 a particularly large change occurred in the mixed layer rising from –0.8˚ to 0.7˚C. The temporal variation below the main thermocline became quite small in this polar region (a few tenths of a degree Celsius) compared to the temperature variability in the mixed layer as well as compared to Aoki's (1997) observation at the corresponding depth. Such small variation may not be significant since it is close to the error introduced by the lateral separation of the cruise tracks.

The large interannual variability in the mixed layer and main thermocline temperature warrants an examination of the temperature structure in the upper ocean including the mixed layer and T_{min} layer. From March 1998 to March 2002 the mixed layer depth increases about 30m and T_{min} depth increases about 20m. Accompanying these increases, we see that the mixed layer temperature decreases about 1˚C while T_{min} temperature increases about 1.5˚C for the same period. As a result, the enthalpy associated with the heat content above the seasonal thermocline decreases with time (Figure 10). The striking linear variation of the mixed layer, T_{min} temperature and depth (Figure 10) may have resulted from the sparseness of the samples. The linear variations are likely a part of the interannual and/or decadal variability and contribute to long-term trends in the upper ocean. However, because of their large magnitudes it is unlikely that the slopes of the linear variations reflect the strength of the long-term trend in the upper ocean. The T_{min} depth is in general agreement with Gordon and Molinelli's (1982) description, although the T_{min} temperature is considerably higher than the one they reported, which was below the –1.0˚C in this area.

To better understand the interannual variability in the upper ocean, including the mixed layer and T_{min} layer, the surface forcing is investigated. This polar area is seasonally covered by sea ice. Winter sea ice reduces the heat and momentum fluxes between the atmosphere and ocean. After the ice melts, the upper ocean is exposed to the atmosphere and the surface forcing directly influences its structure. Therefore, the length of the ice-free period since the previous winter and the strength of surface wind stirring during this period are two major factors determining the temperature structure in the upper ocean. The ice-free period was calculated from the "last ice" day of the winter to prior to each XBT/XCTD survey using the daily sea ice concentration data. It increases from 91 days in 1998 to 113 days in 2002. In addition, friction velocity cubed ($u_*^3 = (\square/\square)^3$), a parameter associated with the surface kinetic energy flux, was calculated using NCEP/NCAR reanalysis daily surface winds and then averaged over the ice-free period. The mean u_*^3 also increases with time during our study period.

The data suggests that when the length of the ice-free period and the strength of u_*^3 increase we also see an increase in the depth of the mixed layer and T_{min} layer. At the same time, the mixed layer temperature becomes colder and T_{min} layer temerature becomes warmer. As a result, the enthalpy above the seasonal thermocline becomes reduced (Figure 11). Both an increase in ice-free period and increase in surface wind stirring contribute to enhanced turbulent mixing in the mixed layer, which entrains more cold water from the T_{min} layer, resulting in greater mixed layer depth and colder mixed layer temperature. Presumably T_{min} has warmed from the freezing point since the previous winter by diffusive processes eroding the warmer waters above and below the T_{min} layer (Toole, 1981). The rate of warming depends on the strength of diffusive processes after the forcing for the winter mixed layer stops. Apparently the stronger surface mixing and longer ice-free period (which transfers to a longer period since the forcing for the winter mixed layer stops) enhance internal diffusive processes that cause T_{min} temperature to erode further away from the freezing point (warmer T_{min} temperature).

Although our analysis suggests a causal relationship between surface forcing and upper ocean thermal structure variability, the limited sampling prevents us from evaluating the significance of the relationship and isolating the contribution from each factor. To further examine this relationship, we also compared our data with historical hydrographic data in the National Oceanography Data Center (NODC), in which we found seven cruises within our study area in February and March from 1978 to 1996. The mean temperature profile for each cruise was generated by averaging available data (from more than three profiles for most cruises). The T_{min} depth and mixed layer temperature from our observations are within the historical range of variability, while the T_{min} temperature and mixed layer depth are near extreme values of these historical observations. Particularly in 2000 and 2002 the T_{min} temperature reaches the historical high, and mixed layer depth in year 2002 reaches the historical maximum (data are not shown here). Although the linear relationships in Figure 10 do not necessarily represent the strength of the trend in the thermal structure of the upper ocean, the extreme values in the earlier 21st century do contribute to long-term trends in T_{min} temperature and mixed layer depth. To utilize available satellite sea ice observations and simulated surface winds from reanalysis products with higher quality (1980s and later), we selected six cruises (one from the 1980s and five from the 1990s) and calculated associated ice-free periods and the mean u_*^3. The causal relationships between surface forcing and the upper ocean thermal structure observed in our data hold for broader ranges in the historical data (Figure 12). Moreover, the relationship with u_*^3 seems to be more profound (with steeper slopes and less scatter) than that with ice-free periods. Apparently the surface forcing, not oceanic fluctuation, determines the upper ocean thermal structure since the lateral thermal gradient in the upper ocean is relatively small in this polar region.

7. Summary

Although the time series of XBT/XCTD surveys in the southeast Indian Ocean are still too short to address the interannual variability of the upper ocean, these four transects have revealed some new aspects of oceanic temporal variation in this data-sparse region.

The three XBT/XCTD surveys in November 1998, March 2000 and March 2002 clearly identify the major oceanic fronts: the subtropical front, subantarctic front and polar fronts. Definitions, locations and main T-S characteristics of these fronts are summarized in Table 1. Identified frontal positions agree with earlier studies in general. The differences between our frontal positions and earlier studies most likely reveal temporal variation of these fronts. The frontal variations for the STF and SAF that we observed are relatively small compared to the frontal variability along 110˚E observed by Nagata et al. (1988). Moreover, a double PF structure is found southeast of the Kerguelen Plateau in these three transects. The two PFs are separated by a few degrees of latitude. The primary PF is characterized by strong horizontal temperature and salinity gradients extending deep in the water column, while the secondary PF is identified by the 2˚C isotherm at T_{min} depth and has a relatively shallow frontal expression.

Dynamic height across the ACC was calculated using XCTD data from the transects in 2000 and 2002. Although the temporal variation of the total transport across the ACC is rather small in these two years, the higher sample density in 2002 reveals more detailed structure of the ACC: two jet streams associated with the SAF and primary PF are embedded within the broad ACC. The surface speed of these two jets is about five times that of the mean ACC speed outside of the jets.

Strong temporal variability is found in the upper ocean thermal structure in the polar region southeast of the Kerguelen Plateau. The mixed layer and T_{min} depths co-vary positively whereas the mixed layer and T_{min} temperatures co-vary negatively. The depths of the mixed layer and T_{min} layer increase with time. The mixed layer temperature decreases while the T_{min} temperature increases at the same time. These variations in the temperature structure cause the upper ocean heat content to decrease with time. In addition, surface forcing, represented by the ice-free period prior to each XBT/XCTD sampling and surface wind stirring measured by the mean friction velocity cubed (u_*^3) during the ice-free period, increases from 1998 to 2002. Our analysis suggests the following mechanisms linking surface forcing from the atmosphere and cryosphere to the variability of the upper ocean thermal structure. The longer ice-free period and the stronger the wind stirring during this period cause enhanced turbulent mixing, which results in the greater mixed layer depth and more entrainment from the T_{min} layer to the mixed layer. These two surface processes also enhance internal diffusive processes that erode the T_{min} layer by mixing warmer waters above and below the T_{min} layer, resulting in increasingly warmer T_{min} temperature. Apparently the upper ocean thermal structure in this polar region is strongly influenced by the surface forcing, particularly by the strength of wind stirring.

The time series of the upper ocean thermal structure are crucial in understanding climate changes in the coupled atmosphere-ocean-ice system. International collaboration and ship-of-opportunity surveys make it feasible to repeatedly sample this remote but important area. Our observations have begun to fill some gaps in the data-sparse Southern Ocean. Our analysis of the initial data begins to reveal the upper ocean variability and contributes to understanding the roles of the atmosphere and cryosphere in determining the oceanic structure.

Acknowledgements. The authors thank A. Gordon and S. Jacobs for helpful discussions, and C. Li for computational assistance. We also thank the Chinese Arctic and Antarctic Administration for supporting the field sampling. Special thanks go to the captain S.

Yuan of R/V Xuelong and Y. Lou from Polar Research Institute of China for assistance with XBT/XCTD data collections. Sea Ice concentration data were provided by the National Snow & Ice Data Center. The work was accomplished under the support of National Science Foundation with the grant OPP9980632, and National Natural Science Foundation of China with the grant 49836010. Lamont-Doherty Earth Observatory contribution number 6539.

References

Aoki, S., 1997. Trends and interannual variability of surface layer temperature in the Indian Sector of the Southern Ocean observed by Japanese Antarctic Research Expeditions. J. of Oceanography, 53, 623-631.

Belkin, I. M. and A. Gordon, 1996. Southern Ocean fronts from the Greenwich meridian to Tasmania, *J. Geophys. Res.,* 101, 3675-3696.

Comiso, J. 1999, updated 2002. Bootstrap sea ice concentrations for NIMBUS-7 SMMR and DMSP SSM/I. Boulder, CO, USA: National Snow and Ice Data Center. Digital media.

Conkright, M, S. Levitus, T. O'Brien, T. Boyer, J. Antonov, and C. Stephens, 1998. World Ocean Atlas 1998 CD-ROM Data Set Documentation. Tech. Rep. 15, NODC Internal Report, Silver Spring, MD, 16pp.

CSIRO Cookbook for Quality Control of Expendable Bathythermography (XBT) Data, 1993, CSIRO, Australia, pp74.

Gordon, A. L., 1971. Antarctic polar front zone, in Antarctic Oceanology I, *Antarctic Research Series*, edited by J. L. reid, 205-221, AGU, Washington D. C..

Gordon, A. L and E. J. Molinelli, 1982. Thermohaline and chemical distributions and the atlas data set in *Southern Ocean Atlas*, Columbia University Press, New York.

Kalnay, E., M. Kanamitsu, R. Kistler, W. Collins, D. Deaven, L. Gandin, M. Iredell, S. Saha, G. White. J. Woollen, Y. Zhu, M. Chelliah, W. Ebisuzaki, W. Higgins, J. Janowiak, K. C. Mo, C. Ropelewski, J. Wang, A. Lettma, R. Reynolds, R. Jenne, and D. Joseph, 1996. The NCEP/NCAR 40-year reanalysis project, *Bulletin of the American Meteorological Society*, 77: 437-471.

Lewis, E. L., 1980. The practical salinity scale 1978 and its antecedents. *IEEE Journal of Oceanic Engineering*, OE-5 (1), 3-8.

Moore, J. K., M. R. Abbott, and J. G. Richman, 1999. Location and dynamics of the Antarctic polar front from satellite sea surface temperature data. *J. Geophys. Res.,* 104, 3059-3073.

Nagata, Y., Y. Michida, and Y. Umimura, 1988. Variation of position and structures of the oceanic fronts in the Indian Ocean sector of the Southern Ocean in the period from 1965 to 1987, in Antarctic Ocean and Resources Variability, edited by D. Sahrhage, Springer-Verlag, New York, 92-98.

Orsi, A. H., T. Whitworth III and W. D. Nowlin Jr., 1995. On the meridional extent and fronts of the Antarctic Circumpolar Current, Deep-Sea Research, 42 (5)., 641-673.

Park, Y.-H., L. Camberoni, and E. Charriaud, 1993. Frontal structure, water masses and circulation in the Crozet Basin, *J. Geophys. Res.*, 98, 12,361-12,385.

Perkin, R. G and E. L. Lewis, 1980. The practical salinity scale 1978: fitting the data. *IEEE Journal of Oceanic Engineering*, OE-5 (1), 9-16.

Peterson, R. G. and L. Stramma, 1991. Upper-level circulation in the South Atlantic Ocean, *Prog. Oceanogr.*, 26, 1-73.

Rintoul, S. R., J. R. Donguy and D. H. Roemmich, 1997. Seasonal evolution of upper ocean thermal structure between Tasmania and Antarctic, *Deep-Sea Res.*, Part I, 44, 1185-1202.

Rintoul, S. R. and J. L. Bullister, 1999. A late winter hydrographic section from Tasmania to Antarctica, *Deep-Sea Res*. Part I, 46, 1417-1454.

Rintoul, S. R. and S. Sokolov, 2001. Baroclinic transport variability of the Antarctic Circumpolar Current south of Australia (WOCE repeat section SR3). *J. Geophys. Re*., Vol. 106 2815-2832.

Rintoul SR, Sokolov S, Church J, 2002. A 6-year record of baroclinic transport variability of the Antarctic Circumpolar Current at 140 degrees E derived from expendable bathythermograph and altimeter measurements. *J. Geophys. Res-Oceans,* 107 (C10): Art. No. 3155 SEP-OCT.

Roemmich, D., 1983. Optimal estimation of hydrographic station data and derived fields, *J. Physical Oceanography*, 13, 1544-1549.

Sievers, H. A. and W. J. Emery, 1978. Variability of the Antarctic Polar Frontal Zone in Drake Passage – Summer 1976-1977, *J. Geophys. Res.,* 83, 3010-3022.

Sparrow, M. D., K. J. Heywood, J. Brown, and D. P. Stevens, 1996. Current structure of the south Indian Ocean, *J. Geophys. Res.,* 101, 6377-6391.

Sokolov, S. and S. R. Rintoul, 2000. Circulation and water masses of the Southeast Pacific: WOCE Section P11, Papua New Guinea to Tasmania. *J. Marine Res*., 58(2), 223-268.

Sokolov, S. and S. R. Rintoul, 2002. Structure of Southern Ocean fronts at 140E. *J. of Marine System,* 37(1-3), 151-184.

Toole, J, 1981. Sea ice, winter convection, and the temperature minimum layer in the Southern Ocean, *J. Geophys. Res*. 86, 8037-8047.

White B. W. and Peterson R. G., An Antarctic circumpolar wave in surface pressure, wind, temperature and sea ice extent, *Nature*, Vol. 380, 699-702, 1996.

Yuan, X., D. G. Martinson and W. T. Liu, 1999. Effect of air-sea-ice interaction on Southern Ocean subpolar storm distribution. *Journal of Geophysical Research*, 104, D2, 1991-2007.

Yuan, X. and D. G. Martinson, 2000. Antarctic sea ice extent variability and its global connectivity, *Journal of Climate,* **3**, 1697-1717.

Captions

Figure 1. XBT/XCTD sampling locations for four cruises between Fremantle, Australia and Prydz Bay, Antarctica in March 1998, November 1998, March 2000, and March 2002. The topography of the Southern Indian Ocean from ETOPO5 5x5 minute resolution Navy database is displayed in the background.

Figure 2. T/S plot based on the data collected in 2002. Major water masses, the Antarctic Surface Water (AASW), Subantarctic Surface Water (SASW), Subtropical Surface Water (STSW), Circumpolar Deep Water (CDW), and Subantarctic Mode Water (SAMW) are marked along with the STF, SAF and PF.

Figure 3. Temperature distribution along the Fremantle/Prydz Bay transect during Nov. 27 to Dec. 2, 1998 (b). Contour interval is 0.5˚C. Vertical dotted lines indicate the sampling location. Topography along the cruise track is displayed at the bottom. November climatology of wind stress curl along the cruise track is plotted in (a). The November climatological wind stress curl was calculated from NCEP/NCAR reanalysis monthly surface winds from 1975 to 2001.

Figure 4. Temperature (b) and salinity (c) distributions along the Fremantle/Prydz Bay transect during March 5 to 11, 2000, together with the topography along the cruise track. The contour interval is 0.5˚C for temperature and 0.05 for salinity (in practical salinity

scale, unit-less). March climatology of surface wind stress curl from NCEP/NCAR reanalysis (1975-2001) is plotted along the transect in (a).

Figure 5. Same as figure 4 except temperature and salinity data were collected during March 2 to 7, 2002.

Figure 6. The location of primary PF (circles), secondary PF (open circles), SAF (triangles), and STF (squares) derived from the objectively mapped temperature sections in 1998, 2000, and 2002 superimposed on the frontal pattern in the Southern Indian Ocean from BG96. Two-way arrows along 110˚E marked the ranges of interannual variability of the PF, SAF and STF based on 22 years of Japanese XBT observations (Nagata et al., 1988).

Figure 7. (a) Dynamic height relative to 750m along the Fremantle/Prydz Bay transect calculated from XCTD data during March 2000 (dashed line) and March 2002 (solid line). The units are m^2/s^2. Potential density distributions in 2000 (b) and 2002 (c) are also plotted.

Figure 8. The temperature profiles in the polar region bounded by 60˚-64˚S and 78˚-83˚E from March 1998 (a), March 2000 (b), and March 2002 (c) cruise.

Figure 9. The 10m-mean temperature centered at 50, 100, 150, 200, 300, 400, 500 and 600m based on the regional mean profile in the polar region as a function of time. The

regional mean profiles were calculated by averaging the profiles in Figure 8 for each year.

Figure 10. Mixed layer depth (circles), T_{min} layer depth (crosses) (a), mixed layer temperature (circles), T_{min} layer temperature (crosses) (b), and the upper ocean enthalpy (c) as functions of time.

Figure 11. Enthalpy (top), mixed layer (circles)/T_{min} layer (crosses) depth (middle) and temperature (bottom) as functions of ice-free days (left column) and the mean friction velocity cube during the ice-free period (right column).

Figure 12. Same as in figure 11 except including historical hydrographic data from NODC. Heavy symbols mark the observations from our XBT/XCTD surveys.

Table 1. Definitions, locations, and main characteristics of the fronts in the southeast Indian Ocean

	Criterion	Latitude	Cross-front Temperature range	Cross-front salinity range
STF	High temperature gradient across 13°-16°C	39°S (1998) 41.8°S (2000) 40°S (2002)	13°-15°C at the surface	34.8-35.0 at the surface
SAF	Southern-most extent of S_{min} and SAMW	45°S (1998) 44.5°S (2000) 46°S (2002)	6°-10°C below 200 m	34.2–34.7 below 200 m
Primary PF	High temperature gradient between 3° to 6°C	49°S (1998) 50.3°S (2000) 51.8°S (2002)	3°-6°C below 200 m	34.4–34.6 below 400 m
Secondary PF	T_{200}=2°C 2°C isotherm at T_{min} layer	53.5°S (1998) 52.5°S (2000) 54.5°S (2002)	3°-4°C at the surface	

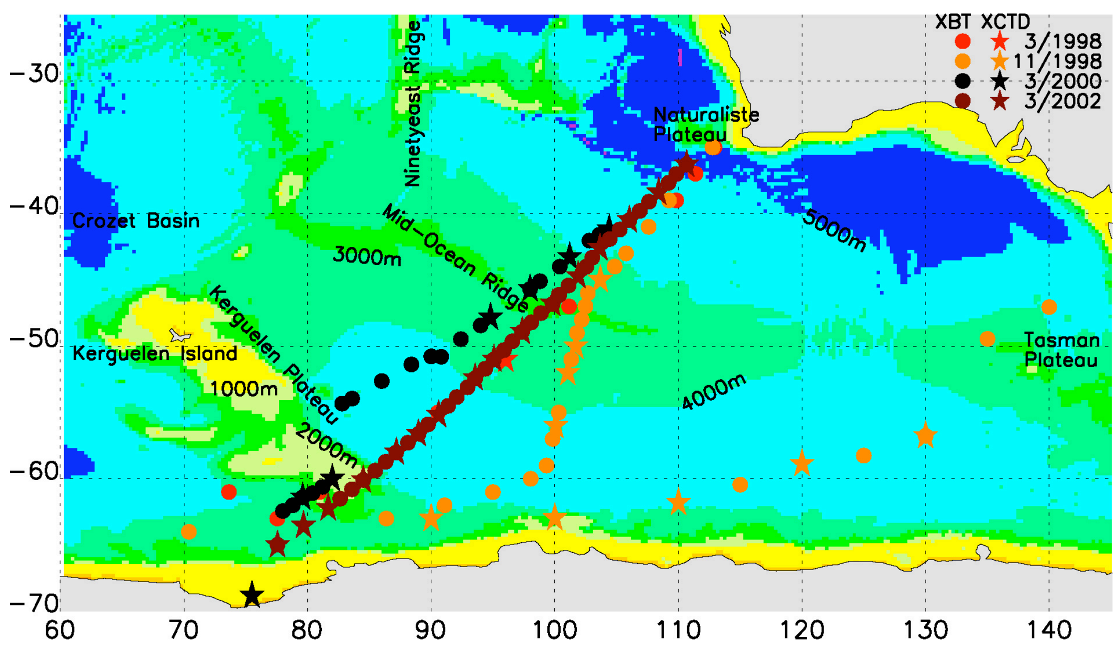

Figure 1

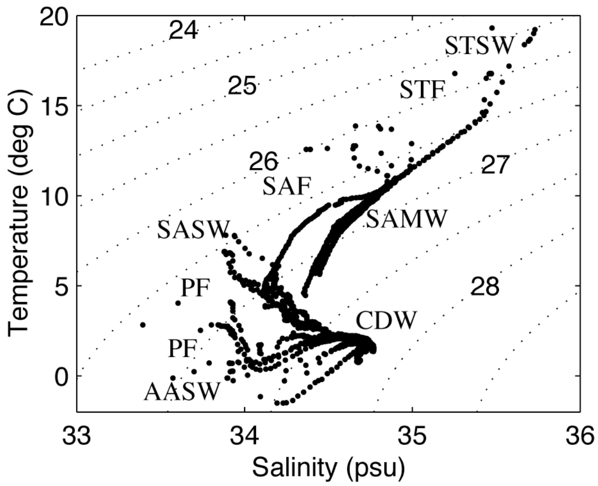

24
25
26
27
28
STSW
STF
SAF
SAMW
SASW
PF
CDW
PF
AASW
Temperature (deg C)
Salinity (psu)
20
15
10
5
0
33
34
35
36

Figure 2

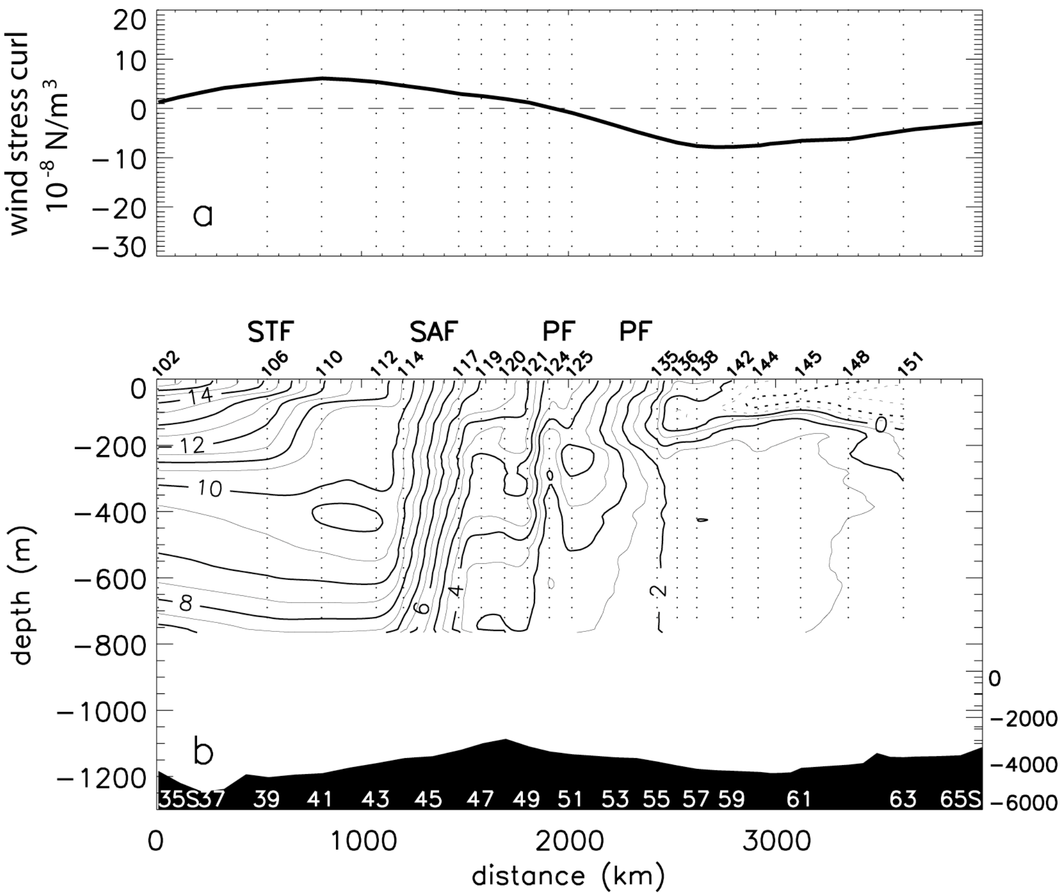

Figure 3

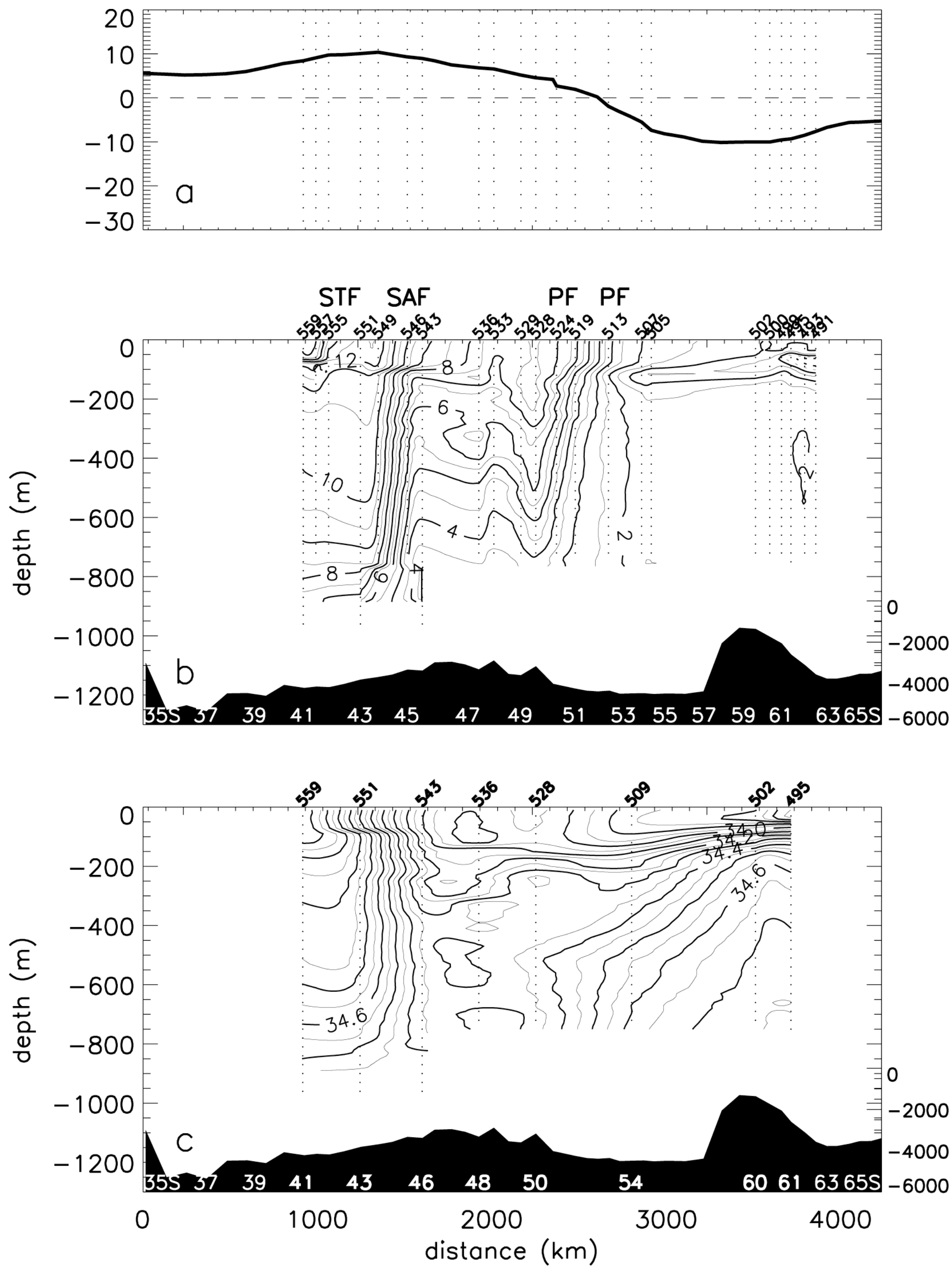

Figure 4

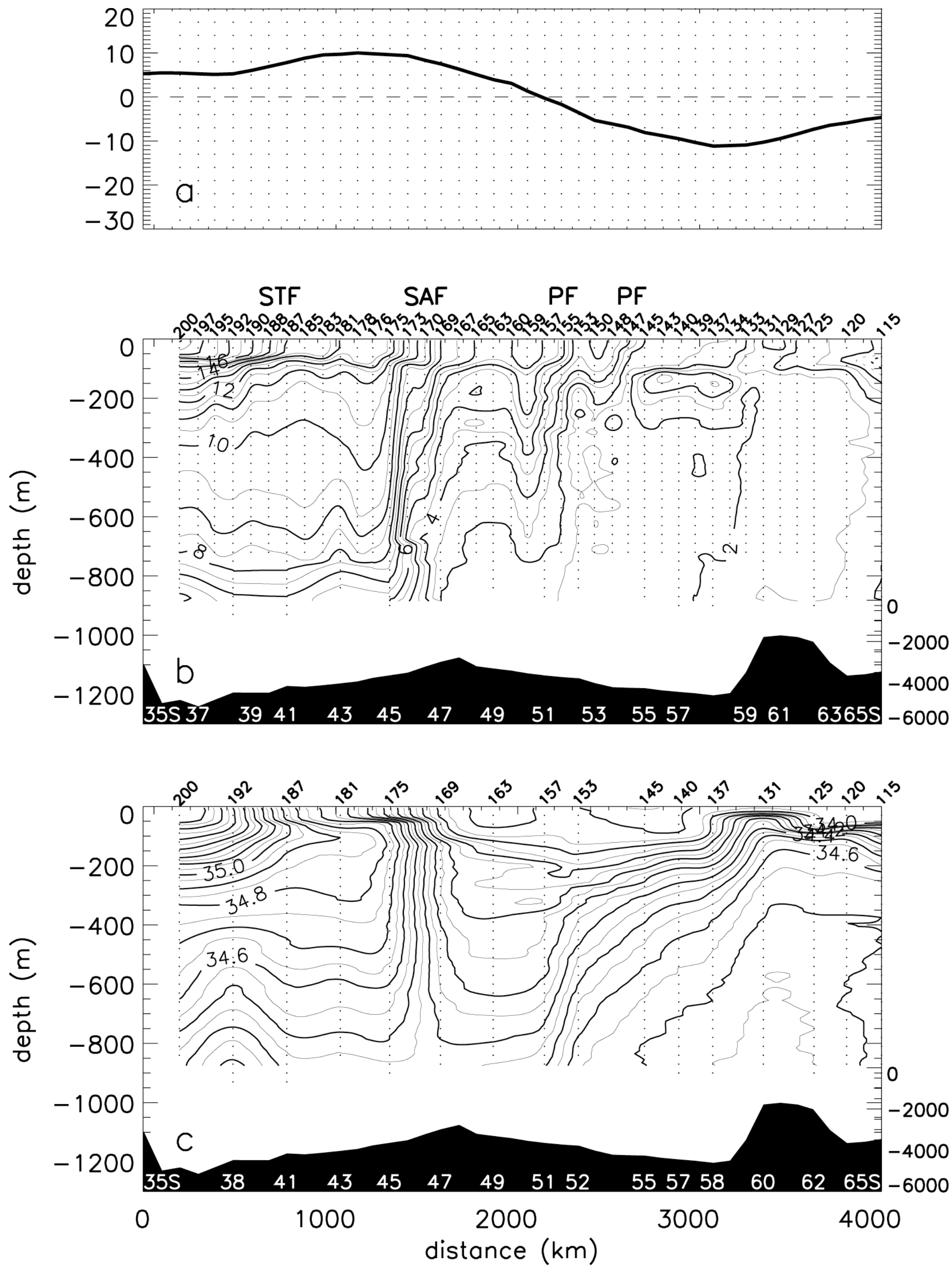
a
b
c
STF
SAF
PF
PF
depth (m)
distance (km)
35S
65S
14
12
10
8
6
4
2
35.0
34.8
34.6
34.0

Figure 5

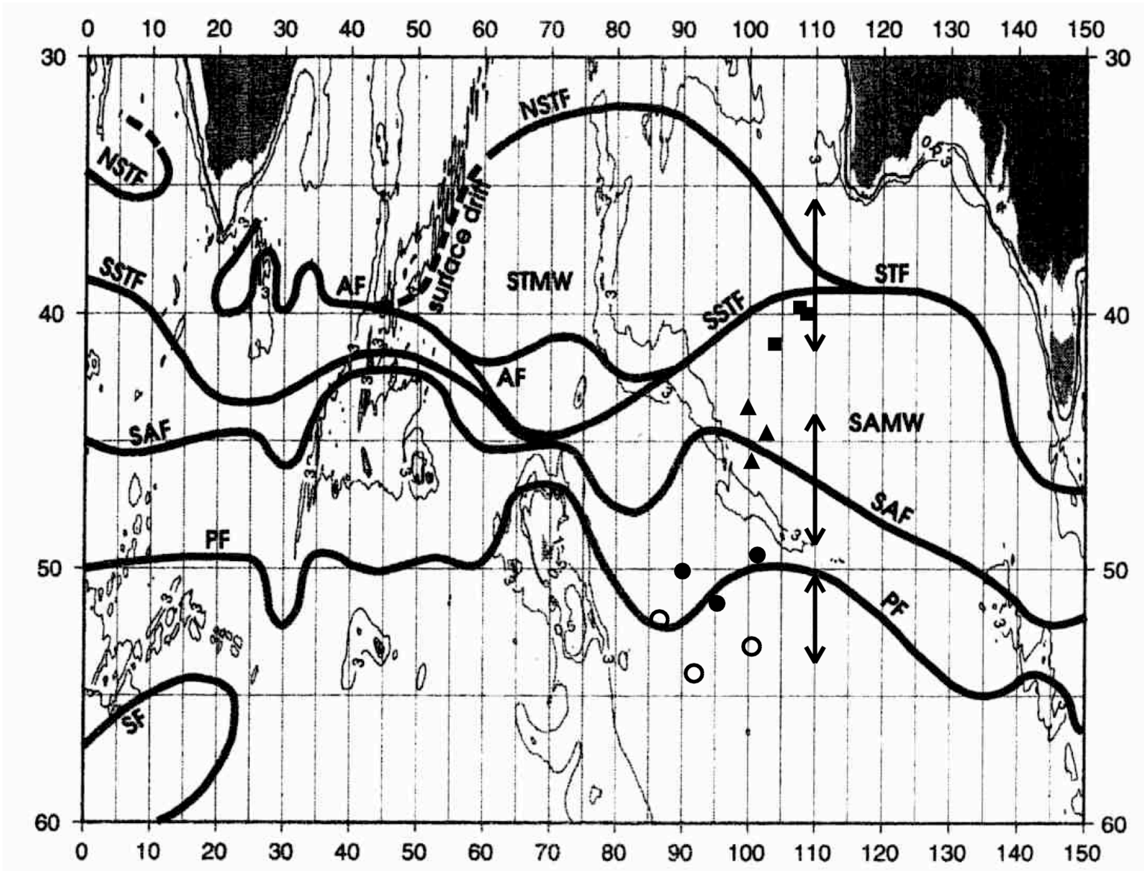

NSTF
NSTF
SSTF
AF
surface drift
STMW
AF
SSTF
STF
SAMW
SAF
SAF
PF
PF
SF

Figure 6

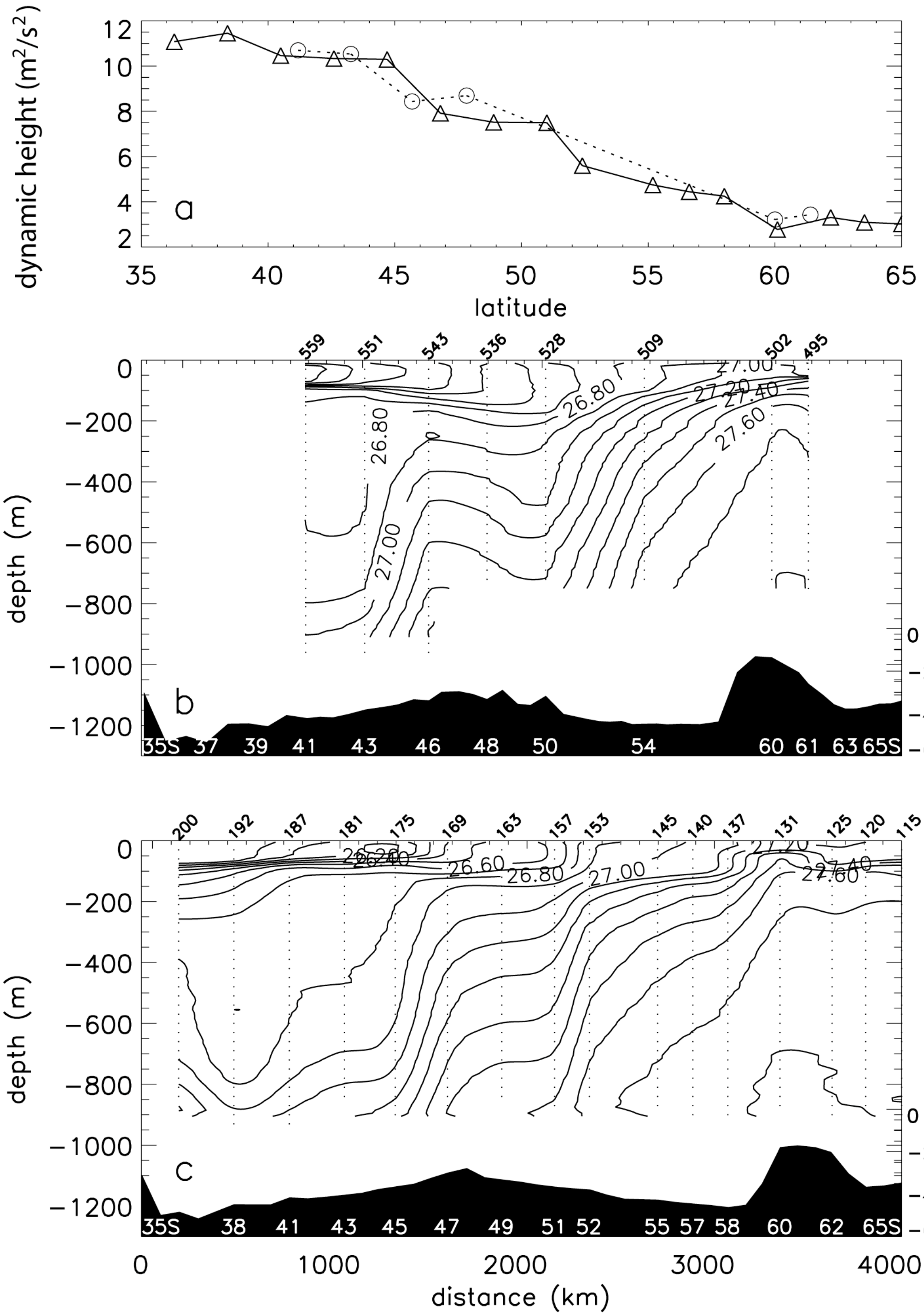

dynamic height (m²/s²)
latitude
a
depth (m)
b
c
distance (km)
26.80
27.00
27.20
27.40
27.60
26.60
559 551 543 536 528 509 502 495
200 192 187 181 175 169 163 157 153 145 140 137 131 125 120 115
35S 37 39 41 43 46 48 50 54 60 61 63 65S
35S 38 41 43 45 47 49 51 52 55 57 58 60 62 65S

Figure 7

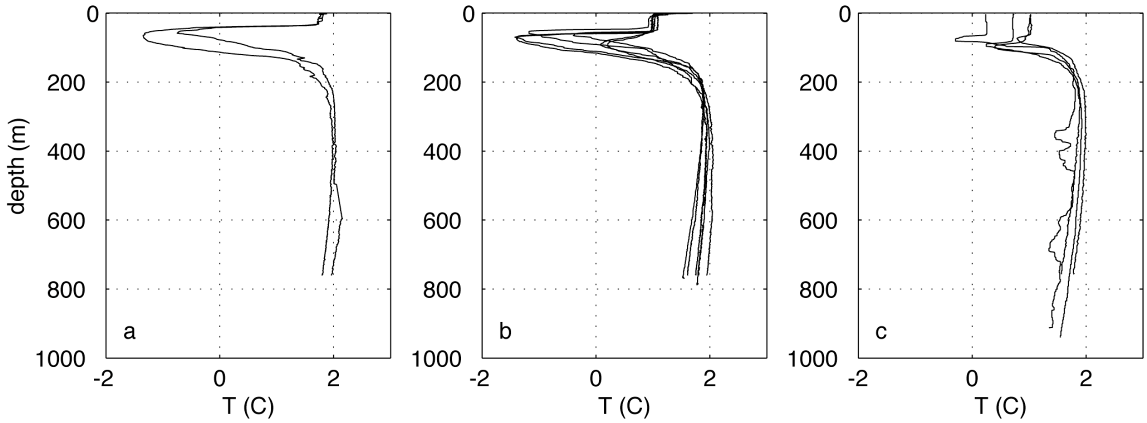

Figure 8

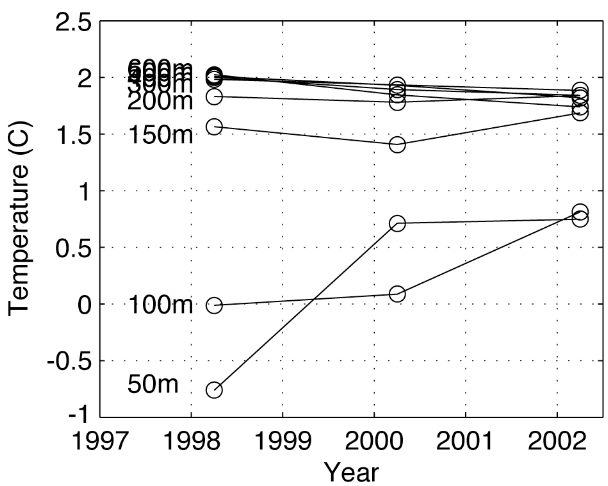

Figure 9

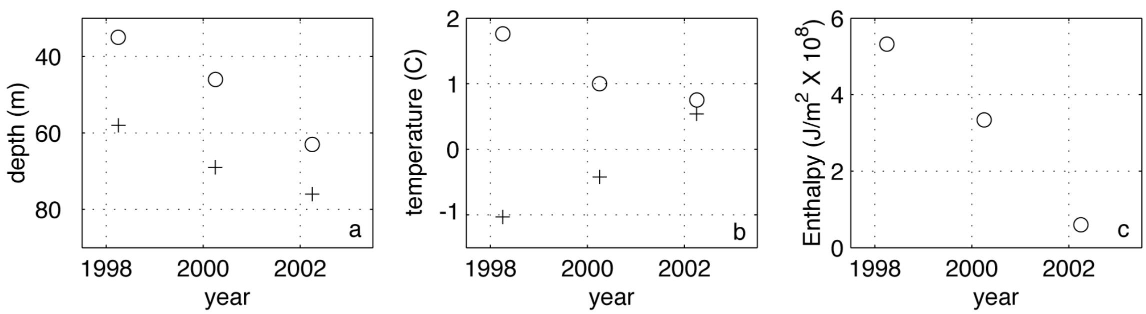

Figure 10

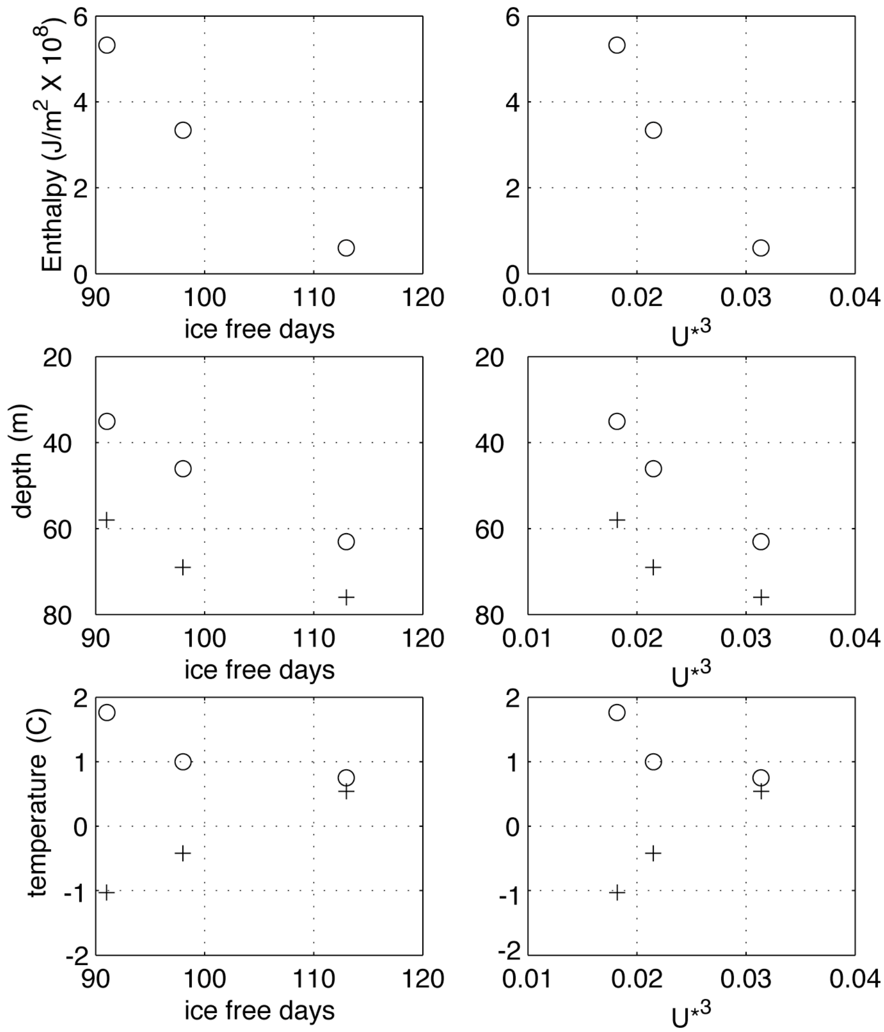

Figure 11

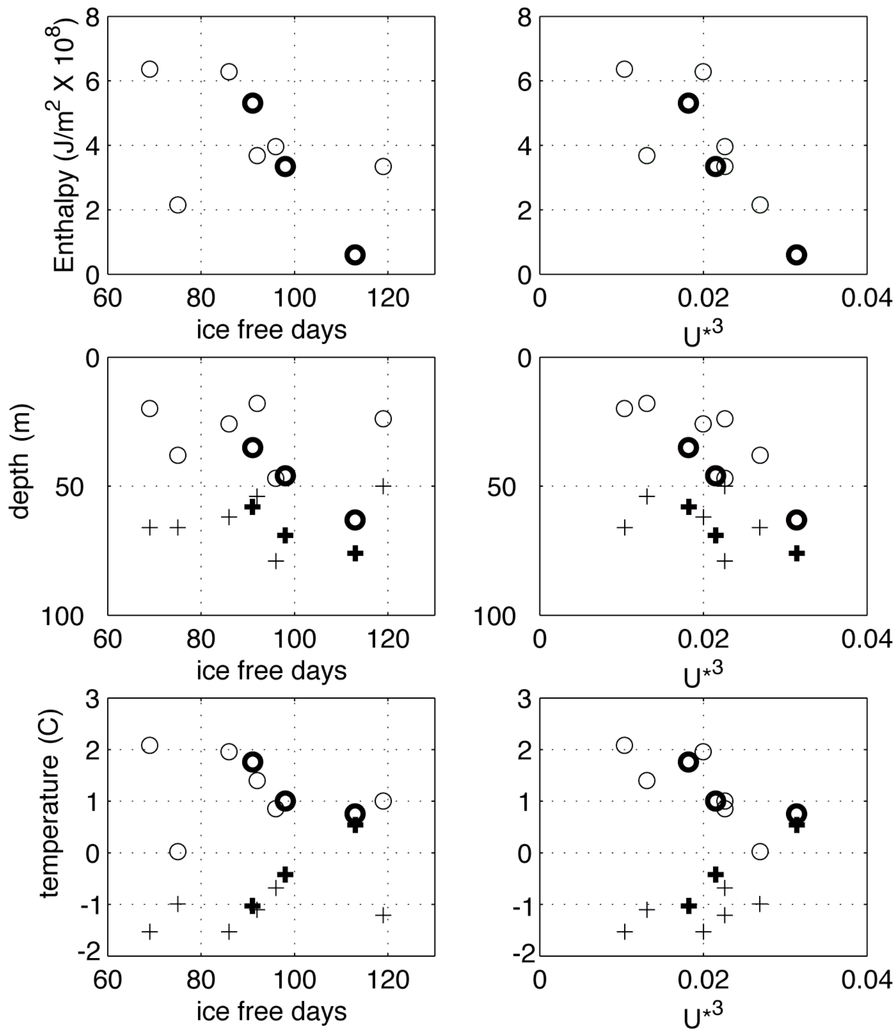

Figure 12